PCCP

PAPER

Cite this: *Phys. Chem. Chem. Phys.*, 2015, **17**, 27758

Electronic storage capacity of ceria: role of peroxide in Au_x supported on $CeO_2(111)$ facet and CO adsorption†

Yinli Liu,[a] Huiying Li,*[a] Jun Yu,[a] Dongsen Mao[a] and Guanzhong Lu*[ab]

Received 11th June 2015,
Accepted 15th September 2015

DOI: 10.1039/c5cp03394b

www.rsc.org/pccp

Density functional theory (DFT+U) was used to study the adsorption of Au_x (x = 1–4) clusters on the defective $CeO_2(111)$ facet and CO adsorption on the corresponding Au_x/CeO_{2-x} catalyst, in this work Au_x clusters are adsorbed onto the CeO_{2-x} + superoxide/peroxide surface. When Au_1 is supported on the $CeO_2(111)$ facet with an O vacancy, the strong electronegative $Au^{\delta-}$ formed is not favorable for CO adsorption. When peroxide is adsorbed on the $CeO_2(111)$ facet with the O vacancy, Au_x was oxidized, resulting in stable Au_x adsorption on the defective ceria surface with peroxide, which promotes CO adsorption on the Au_x/CeO_{2-x} catalyst. With more Au atoms in supported Au_x clusters, CO adsorption on this surface becomes stronger. During both the Au being supported on CeO_{2-x} and CO being adsorbed on Au_x/CeO_{2-x}, CeO_2 acts as an electron buffer that can store/release the electrons. These results provide a scientific understanding for the development of high-performance rare earth catalytic materials.

1. Introduction

Ceria supported gold (Au/CeO_2) catalysts have become one of the hottest systems in catalysis, being widely applied to many important processes, such as CO oxidation,[1–3] water-gas shift (WGS) reactions,[4–7] methanol synthesis,[8] hydrocarbon oxidation,[9] NO reduction,[10–12] and automotive exhaust purification.[13]

Since the pioneering work (Au/oxides) of Haruta,[14] ceria supported gold catalysts and their role in CO oxidation have been drawing extensive interest experimentally and theoretically. Contributions from the literature can be summarized in three major aspects: (i) the size-dependent catalytic activity of supported Au catalysts has been extensively studied, and supported gold clusters of sizes smaller than 5 nm exhibit very high surface reactivity.[15–21] (ii) $Au^{\delta+}$ species stabilized on an oxide can act as active sites, while $Au^{\delta-}$ ions are inactive for CO adsorption.[22,23] The experimental results are consistent with theoretical research results.[1,6,24,25] Those studies reveal that oxygen vacancies increase the adsorption or binding of Au on the ceria surface.[4,26,27] However, an interaction of Au with oxygen vacancies tends to form negatively charged Au,[24,28] which is inactive for CO adsorption. Thus, how to transfer the charge from the Au cluster to some other species so that the Au will be active for CO interaction is an important topic. (iii) The role of ceria:[29–31] the nanocrystalline CeO_2 support can enhance the activity of Au for CO oxidation.[29] The reactive oxygen on nano Au/CeO_2 crystallite surfaces exists in the form of superoxide (O_2^-) and peroxide (O_2^{2-}) ad-species during CO oxidation at low temperature.[23,32] In an oxygen atmosphere, superoxide and peroxide are two kinds of important oxygen species on the $CeO_2(111)$ surface, which can be characterized by electron paramagnetic resonance (EPR), Raman and FT-IR spectroscopies.[23,33–37] We found that on the reduced $CeO_2(111)$ facet, oxygen adsorbed on a surface vacancy forms a peroxide, and oxygen adsorbed on a subsurface vacancy forms a superoxide according to density functional theory (DFT+U) calculations.[38] Fabris and Huang studied the adsorption behaviors of superoxide on the $CeO_2(111)$ with an O vacancy and $CeO_2(110)$ facets.[39] Using a DFT+U approach, Teng *et al.* investigated the electronic properties of superoxide and peroxide species on a partially reduced $CeO_2(111)$ model catalyst.[40] They also found that CO can be directly oxidized to CO_2 by the superoxide without an energy barrier, while carbonate can form when CO reacts with peroxide. After O_2 is adsorbed on a $Au_3/CeO_2(110)$ surface, we found, O_2^- species could form.[41]

Theoretical study with DFT+U is a powerful tool to understand the catalysis or catalytic reaction mechanism, and can be adopted to study the vacancy, metal doping, and adsorption/reaction mechanism on the ceria catalyst.[42–51] Although theoretical

[a] *Research Institute of Applied Catalysis, Shanghai Institute of Technology, 100 Haiquan Road, Shanghai 201418, P. R. China. E-mail: hyli@sit.edu.cn; Fax: +86-21-60877231*

[b] *Key Laboratory for Advanced Materials and Research Institute of Industrial Catalysis, East China University of Science and Technology, 130 Meilong Road, Shanghai 200237, P. R. China. E-mail: gzhlu@ecust.edu.cn; Fax: +86-21-60879111*

† Electronic supplementary information (ESI) available: Structures and charge density differences for $CeO_2(111)$ facet containing single O vacancy (Fig. S1), peroxide, superoxide, and both peroxide and O vacancy (Fig. S2), and structures of Au_3–$(PO_2)_2$–V_1 and Au_4–$(PO_2)_4$–V_2 and CO oxidation on them (Fig. S3). See DOI: 10.1039/c5cp03394b

studies of Au/CeO_2 as mentioned above provide plenty of information, there are still two major basic challenges requiring more insight: (1) how to make gold clusters adhere well on the ceria surface; (2) what is the role of the Ce f-orbit during Au adsorption on ceria and CO adsorption over the surface of Au/ceria. Therefore, using DFT+U methods, we studied in detail the influence of the O vacancy, peroxide and superoxide species on the gold adsorption on ceria and CO adsorption on the resulting $Au/CeO_2(111)$ structure. We try to provide deeper insights into the origin of Au_x cluster adsorption on the CeO_2 surface, the electron transfer mechanism and how CeO_2 acts as an electron buffer.

This work is organized as follows. The calculation details are mentioned in Section 2. The interactions of Au_x clusters with the O vacancy, peroxide and superoxide on the $CeO_2(111)$ facet are studied in Section 3, including the CO adsorption on the surface. Finally, the conclusions are summarized in Section 4. The results show that the adsorbed peroxide can promote the adsorption of Au_x on ceria and CO adsorption on the Au_x/CeO_{2-x} catalyst, and CeO_2 acts as an electron buffer during the adsorption process.

2. Computational details

The calculations were carried out within the generalized gradient approximation with the VASP.[52,53] The project-augmented wave (PAW) method[54,55] was used to represent the core–valence interaction. The valence electronic states were expanded in plane-wave basis sets with an energy cut-off at 500 eV. The density functional theory (DFT+U) method[50,51,56] was used to treat the highly localized Ce 4f state. The value of $U = 5.0$ eV was adopted in this work, which is the same value as most of the literature on Au/CeO_2 systems.[57–64]

Being different from the works of Branda *et al.*,[49,50] the ceria surfaces were modelled by a p(3×4) unit cell with three CeO_2 layers and a vacuum between slabs of 14 Å. The bottom CeO_2 layer was fixed and all others atoms were relaxed, in which the force threshold was set to 0.02 eV $Å^{-1}$. Monkhorst–Pack mesh of ($1 \times 1 \times 1$) was used for the *k*-point sampling.

In the optimization process, adsorption energies were measured by the following formula, $E_{ads} = -(E_{tot} - E_{sub} - E_x)$, where E_{tot} is the total energy of the combined system, E_{sub} is the energy of the substrate alone, and E_x is the total energy of the adsorbates in the gas phase.

In this work, the Bader charge analysis was utilized for better understanding the electron transfer mechanism of Au_x clusters after being supported on the CeO_2 surface. Like the adsorption energy equation, the difference charge density has been evaluated with the expression: $\Delta\rho(r) = \rho_{tot}(r) - \rho_{sub}(r) - \rho_x(r)$, where $\rho_{tot}(r)$, $\rho_{sub}(r)$ and $\rho_x(r)$ are the charge densities of the whole system, isolated substrate, and adsorbate, respectively.

3. Results and discussion

Herein, we first studied a single Au atom adsorption on the $CeO_2(111)$ facet containing oxygen vacancies, peroxides and superoxides, as well as CO adsorption on the $Au_1/CeO_2(111)$ facet. Structure, charge density difference, adsorption energy and the Bader charge were discussed in detail to understand the electron transfer mechanism during either Au absorption on the CeO_2 surface or CO adsorption on the $Au_1/CeO_2(111)$ surface. Then, we extended this study to Au clusters, *i.e.* Au_x ($x = 2$–4), to gain further insight for more practical catalysts and catalysis. The various structures of Au adsorption on the CeO_2 surface were defined as Au_x–$(PO_2)_y$–$(SO_2)_z$–V_m–$(SV)_n$, where PO_2, SO_2, V and SV represent peroxide, superoxide, surface oxygen vacancies and sub-surface oxygen vacancies respectively, and y, z, m and n are the number of each.

3.1. Au_1 adsorption on the $CeO_2(111)$ facet and CO adsorption on Au_1/CeO_2

The single Au atom adsorbed at the top site of surface oxygen on the clean $CeO_2(111)$ facet (Au_1–O-t) is shown in Fig. 1a. The Au–O bond length and the calculated adsorption energy are 1.99 Å and 0.98 eV (Table 1) respectively, which aligns well with the reported results (2.00 Å and 1.04 eV, respectively).[24] This result indicates a weak adsorption of the single Au atom on the clean CeO_2. A positively charged $Au^{\delta+}$ adatom and a reduced Ce^{3+} ion were found *via* the charge density difference of Au_1–O-t (Fig. 1b). The positively charged $Au^{\delta+}$ was further validated by computing the Bader charge (+0.28*e*, Table 1). Based on these results, we may explain this adsorption process: oxygen on the CeO_2 surface oxidizes Au to form the Au–O bond, thus the electron transfers from the neutral Au atom to the Ce surface by Au–O bond, forming Ce^{3+}. This process can be simply described as follows:[65] $Au - e \rightarrow Au^{\delta+}$, $Ce^{4+} + e \rightarrow Ce^{3+}$.

Although the Au_1 adsorption here is weak and has no practical application, we would like to study further CO adsorption on this positively charged Au (Au_1–O-t surface). As shown in Fig. 1c, the C–O bond length is 1.15 Å, and the distance between the C atom and the Au is 1.88 Å. The charge density difference (Fig. 1d) shows that the Ce^{3+} ion is not charged and the charge of Au is still positive. As shown in Bader charge analysis of Table 1, the charge of $Au^{\delta+}$ is increased from +0.28*e* to +0.51*e* after CO adsorption and CO Bader charge is −0.09*e*, indicating a further electron transferred from the Au atom to CO. Based on this positive charge of Au, the calculated CO adsorption energy is 2.52 eV (Table 1), a strong adsorption.

It was reported that, oxygen vacancy can stabilize Au_x clusters on the reduced $CeO_2(111)$ facet,[6,24] which is our next interest in addition to the clean surface. The structure or spin density of the $CeO_2(111)$ facet containing a single O vacancy is shown Fig. S1 (ESI†), two excess electrons are localized at two Ce ions, which is consistent with our previous calculation.[38] As seen in Fig. 1e for the adsorption of Au_1 on a $CeO_2(111)$ facet with one oxygen vacancy (Au_1–V_1), the Au_1 atom is anchored on the oxygen vacancy at a distance of 1.26 Å, and three Au–Ce bonds are 3.16, 3.16 and 3.21 Å, respectively. The corresponding adsorption energy is 2.32 eV (Table 1), which is much stronger than Au_1 on the clean $CeO_2(111)$ facet. This agrees well with reported results.[66,67] With the aid of the charge density difference analysis for the optimized structure (Fig. 1f), we found the presence of an $Au^{\delta-}$ adatom and one Ce^{3+} for the (Au_1–V_1) case. It was

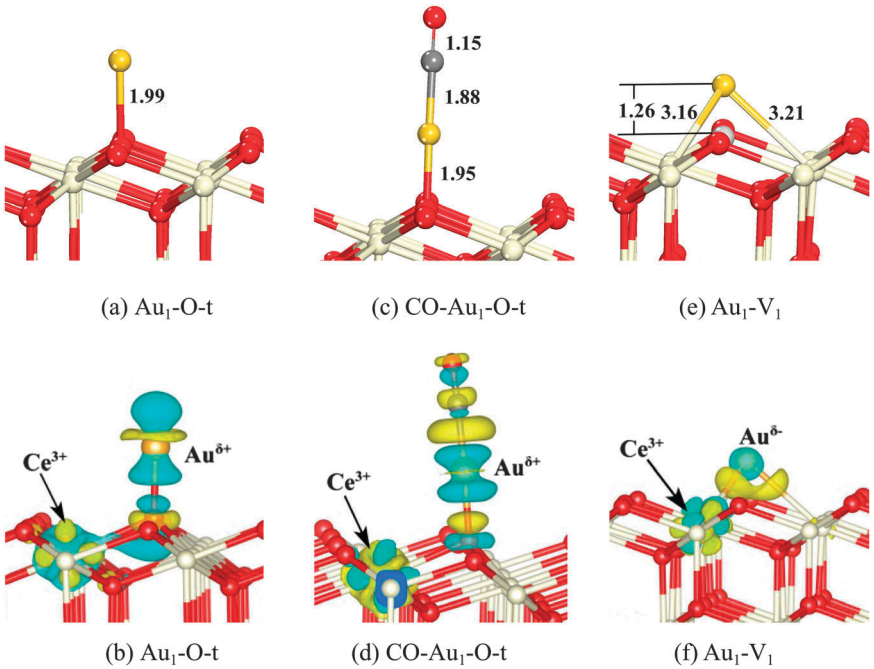

Fig. 1 Optimized structures of (a and e) Au_1 atom on the CeO_2(111) facet and (c) CO adsorption on Au_1/CeO_2(111), and (b, d and f) the corresponding charge density difference. (O, Ce, Au, C atoms are denoted in red, gray, yellow and dark gray, respectively. The O vacancy is represented by balls in light gray. Main bond lengths are reported in Å. Electron accumulation and depletion are represented by yellow and blue areas, respectively. The isosurface value is set as 0.005 e $Å^{-3}$.)

Table 1 The Au_1 or CO adsorption energy (eV) and the Bader charge of Au_1 clusters and CO

	E_{ad}/eV	Au-Bader charge/*e*	CO-Bader charge/*e*
Au_1–O-t	0.98	+0.28	
CO–Au_1–O-t	2.52	+0.51	−0.09
Au_1–V	2.30	−0.62	
Au_1–$(PO_2)_1$	1.75	+0.34	
CO–Au_1–$(PO_2)_1$	1.63	+0.51	−0.05
Au_1–$(SO_2)_1$–$(SV)_1$	1.08	+0.17	
Au_1–$(PO_2)_1$–V_1	2.32	−0.60	

reported that, two Ce^{3+} ions will be generated after formation of one oxygen vacancy.[24,38,55,68,69] These results indicate that an electron transfers from the reduced oxide surface (one of the two Ce^{3+} ions) to the supported Au atom, thus there remains just one Ce^{3+} ion on the reduced surface. The Bader charges in Table 1 show that, the charge of Au is $-0.62e$, showing a very strong electronegativity. Therefore, CO molecules cannot bind with (adsorb onto) the $Au^{\delta-}$ species.[24]

The results above show that, Au_1 adsorption on the reduced surface of CeO_{2-x} with an oxygen vacancy is much stronger than on the clean surface of CeO_2 without an oxygen vacancy. An electron transfers from one of two Ce^{3+} ions to Au, resulting in a very strong electronegativity of Au and CO non-adsorption on this $Au^{\delta-}$ species.

To explain the influence of peroxide and superoxide on the Au adsorption, we studied the adsorption of Au_1 around these oxygen species on the CeO_2(111) facet.

For one peroxide on the CeO_2(111) facet, the Au atom bonds with two O atoms with bond lengths of 2.07 Å ($Au–O_{lattice}$) and 2.09 Å ($Au–O_{peroxide}$), as shown in Fig. 2a. The O–O distance within the peroxide on the adsorbed surface is 1.49 Å, which is bigger than 1.44 Å the original distance (Fig. S2, ESI†). The corresponding Au atom adsorption energy is 1.75 eV (Table 1). An $Au^{\delta+}$ and one Ce^{3+} appeared when studying the charge density difference of this configuration (Fig. 2b), and the charge of $Au^{\delta+}$ was $+0.34e$ from the Bader charge calculation (Table 1).

Based on this structure, CO adsorption on the surface was studied. The optimized structure for CO adsorption on this positively charged $Au^{\delta+}$ ion (Au_1–$(PO_2)_1$ surface) is shown in Fig. 2c, and its adsorption energy was calculated to be 1.63 eV (Table 1). The C–O bond length of adsorbed CO molecule is 1.15 Å, and the distance between the C atom and Au is 1.87 Å, while the Au–O bonds are changed to 2.01 Å ($Au–O_{lattice}$) and 3.06 Å ($Au–O_{peroxide}$). As shown in the charge density difference in Fig. 2b and d, one Ce^{3+} ion exists before and after CO adsorption, and the Bader charge analysis shows Au has a positive charge $+0.51e$ (Table 1). This shows the charge transfers from the $Au^{\delta+}$ adatom to the CO at the Au/CO interface, where the adsorbed $Au^{\delta+}$ ion can act as an active site for CO adsorption on the CeO_2(111) surface with a peroxide.

Au_1 adsorption on the CeO_2(111) facet containing a subsurface O vacancy and a superoxide (Au_1–$(SO_2)_1$–$(SV)_1$) is shown in Fig. 2e. The $Au–O_{superoxide}$ bond length is 2.08 Å and the O–O bond within superoxide is elongated to 1.38 Å from 1.33 Å (Fig. S2, ESI†). As shown in the charge density difference analysis of Au_1–$(SO_2)_1$–$(SV)_1$ (Fig. 2f), there is an $Au^{\delta+}$ ion and Ce^{3+}.

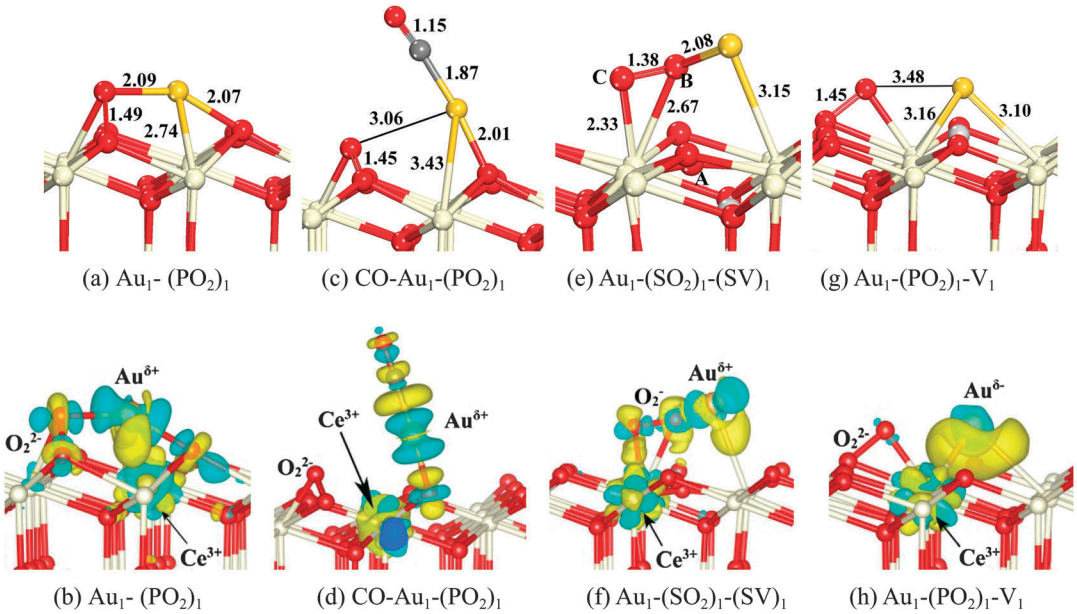

Fig. 2 Optimized structures of (a, e and g) Au_1 atom on the CeO_2(111) facet and (c) CO adsorption on Au_1/CeO_2(111), and (b, d, f and h) the corresponding charge density differences. (O, Ce, Au, C atoms are denoted in red, gray, yellow and dark gray, respectively. The O vacancy is represented by balls in light gray. Main bond lengths are reported in Å. Electron accumulation and depletion are represented by yellow and blue areas, respectively. The isosurface value is set as 0.005 e $Å^{-3}$.)

The reduced Ce^{3+} ion results from the subsurface O vacancy. Furthermore, the Au-d band and the O-2p band of the superoxide are overlapped. The Bader charge analysis shows that Au has a positive charge +0.17*e* (Table 1), due to an electron transfer from the Au atom to the superoxide, forming positively charged $Au^{\delta+}$. The Au_1 adsorption energy was calculated to be 1.08 eV, which is less than Au_1 on the CeO_2(111) surface with a peroxide (1.75 eV). When CO adsorbed onto this surface (Au_1–$(SO_2)_1$–$(SV)_1$), the superoxide structure rearranged to form the structure with a peroxide (CO–Au_1–$(PO_2)_1$, Fig. 2c), because of the instability of the superoxide.[40] The structure rearrangement includes two parts: (1) when CO is close to Au_1, because of the structure effect, the surface oxygen O_A migrates to the subsurface vacancy position, forming the subsurface oxygen and a surface vacancy; (2) once the new surface oxygen vacancy is formed, the nearby oxygen O_B of superoxide easily migrates to the surface vacancy to form peroxide. The CO adsorption energy is 3.19 eV, which may include both CO adsorption energy and structure rearrangement energy. The structure rearrangement energy includes two parts: (1) migration energy from surface oxygen to subsurface oxygen ($O_V \rightarrow O_{SV}$), and (2) migration energy from superoxide to peroxide. In summary, for the CeO_2–$(SO_2)_1$–$(SV)_1$ sample, Au_1 adsorption on its surface is not stable enough compared to adsorption on its structure with peroxide present, because during CO adsorption, its structure was rearranged back to the structure with a peroxide (CO–Au_1–$(PO_2)_1$). Hence in the following discussions, we will focus on the structure with a peroxide (CeO_2–$(PO_2)_1$).

The results above suggest that the presence of a vacancy, peroxide and superoxide helps the adsorption of Au_1 on the CeO_2(111) facet, compared with the clean CeO_2(111) facet, and their corresponding adsorption energy are 2.30 eV, 1.75 eV, 1.08 eV and 0.98 eV, respectively. None of these adsorption energies can overcome Au–Au binding (binding energy is 2.31 eV based on formula $E_{Au-Au} = E(Au)_2 - 2E_{Au}$). Thus there is a question: if the CeO_2(111) facet has the peroxide and O vacancy simultaneously, that is CeO_2–$(PO_2)_y$–V_m, can it assist in the Au adsorption?

The calculated structure and charge density difference for CeO_2–$(PO_2)_1$–V_1 are shown in Fig. S2 (ESI†), and the calculated structure for Au_1–$(PO_2)_1$–V_1 is shown in Fig. 2g. The distance between the Au atom and $O_{peroxide}$ reaches ~3.48 Å, and there is no electron interaction between them. The Au_1 adsorption energy is 2.32 eV in this configuration, which is same as Au–Au binding energy (2.31 eV). This suggests that, when peroxide and oxygen vacancies exist simultaneously on the CeO_2 surface, it is advantageous to the adsorption of gold clusters and it inhibits the reunion on the CeO_2(111) facet. That is to say, when the adsorbed Au migrates from the CeO_2(111) facet toward Au–Au reunion, it should overcome the adsorption energy, *i.e.*, a minimum 2.32 eV, thus this process by which Au atoms migrate to form Au–Au bonds occurs only with difficulty.

The charge density difference analysis of this structure displayed $Au^{\delta-}$ and one Ce^{3+} ion on the surface (Fig. 2h), and the charge transferred from the surface of reduced oxide Ce^{3+} to the Au atom, thus resulting in a negatively charged $Au^{\delta-}$ adatom presented on the surface. The Bader charge analysis shows that the charge of the adsorbed Au is −0.60*e*. Hence CO molecules cannot adsorb on its surface, or bind with $Au^{\delta-}$.

For single Au atom adsorption on the CeO_2(111) facet, we have found that, firstly, the stability of a single Au atom adsorption is arranged in the following order; $(PO_2)_1$–V_1 > V_1 > $(PO_2)_1$ > $(SO_2)_1$–$(SV)_1$ > clean CeO_2(111) facet, where the

combination of peroxide and O vacancy provides the best surface for Au adsorption (even slightly better than Au–Au binding). Secondly, CO could adsorb easily at the positively charged $Au^{\delta+}$. In this way, even on the most promising structure, $(PO_2)_1$–V_1, because of the strongly negatively charged $Au^{\delta-}$, CO molecules cannot adsorb to its surface. Lastly, after Au adsorption on the $CeO_2(111)$ facet with one peroxide, a reduced Ce^{3+} is presented and ceria has a capacity for storing electrons. In the following study on two Au atoms (Au_2), we will continually explore the situation of peroxide adsorbed on the $CeO_2(111)$ facet with and without an O vacancy.

3.2. Au_2 cluster adsorbed on the $CeO_2(111)$ surface and CO adsorption

The optimized structures of Au_2 clusters on reduced $CeO_2(111)$ facets (containing two peroxides or both one oxygen vacancy and two peroxides) and CO adsorption on the Au_2/CeO_2 catalyst, and their charge density difference analyses are shown in Fig. 3. The corresponding adsorption energies and Bader charge data of Au_2 cluster are listed in Table 2.

Table 2 The Au_2 cluster or CO adsorption energy (eV) and the Bader charge of Au_2 clusters

		Au-Bader charge/*e*		CO-Bader charge/*e*
	E_{ad}/eV	Au_A	Au_B	
Au_2–$(PO_2)_2$	1.16	+0.07	+0.05	
CO–Au_2–$(PO_2)_2$	1.20	+0.17	−0.13	−0.05
Au_2–$(PO_2)_2$–V_1-L	2.65	−0.05	−0.12	
CO–Au_2–$(PO_2)_2$–V_1-L	0.51	+0.10	−0.16	−0.02

As shown in Fig. 3a, for the $CeO_2(111)$ facet with two peroxides, Au_2 lies parallel to the surface (Au_2–$(PO_2)_2$). The two gold atoms are anchored by two peroxides, the two bond lengths of Au–$O_{peroxide}$ are 2.14 and 2.37 Å respectively, and the distance between the two Au atoms is 2.58 Å. The corresponding Au_2 adsorption energy is 1.16 eV. Two weakly positively charged Au atoms and one Ce^{3+} were found in the charge density difference of its configuration (Fig. 3b). As shown in Table 2, the Bader charges of two Au atoms are 0.07 and 0.05 respectively. Though the Bader charge of the Au_2 cluster is small, it can be supported

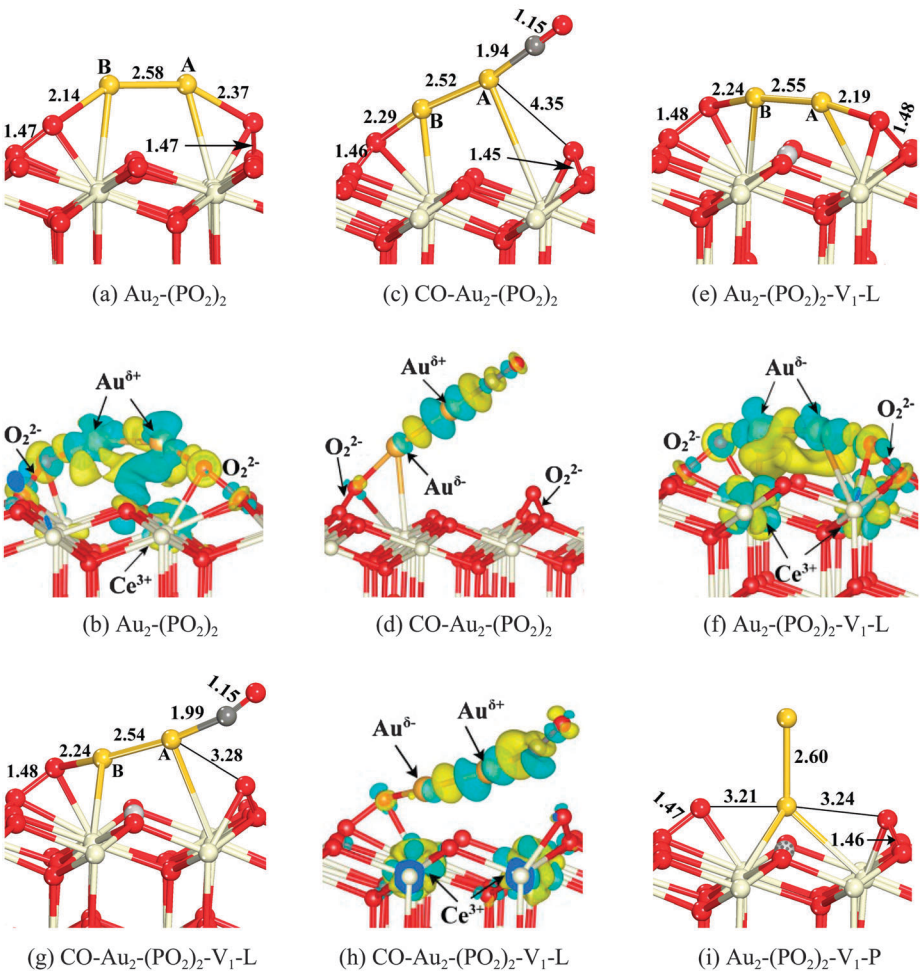

Fig. 3 Optimized structures of (a, e and i) Au_2 clusters on the $CeO_2(111)$ facet and (c and g) CO adsorbed on $Au_2/CeO_2(111)$, and (b, d, f and h) the corresponding charge density differences. (O, Ce, Au, C atoms are denoted in red, gray, yellow and dark gray, respectively. The O vacancy is represented by balls in light gray. Main bond lengths are reported in Å. Electron accumulation and depletion are represented by yellow and blue areas, respectively. The isosurface value is set as 0.005 e $Å^{-3}$.)

by the charge density difference findings. On the basis of Bader charge and charge density difference analysis, we concluded that the Au_2 cluster is oxidized and a reduced Ce^{3+} ion is formed, indicating electron transfer from the Au_2 cluster to the substrate CeO_2.

A CO molecule can chemically adsorb on the surface of $Au_2/CeO_2(111)$ (Au_2–$(PO_2)_2$) with adsorption energy of 1.20 eV, and its optimized structure is shown in Fig. 3c. The distances between Au and $O_{peroxide}$ are changed to 2.29 and 4.35 Å, respectively. After CO adsorption on the Au_2–$(PO_2)_2$ surface, there is a strong charge rearrangement at the contacts of Au/CeO_2 and Au/CO. As shown in Fig. 3d, there is no reduced Ce^{3+} on the $CeO_2(111)$ facet, while the electron clouds of CO and Au_A overlap. The Bader charge results (Table 2) show that, one Au atom (Au_A) in Au_2 cluster is +0.17*e* and another (Au_B far from CO) is −0.13*e*. The Bader charge of CO is −0.05*e*. Combined with the charge density and the Bader charge results, a reasonable deduction can be proposed that a reduced Ce^{3+} ion is formed when Au_2 is attached to the peroxide and the reduced Ce^{3+} ion disappears after CO adsorption. This provides a strong indication of ceria acting as an electron buffer. Here, one Au adatom donates an electron to C in CO and the second Au adatom receives an electron from Ce^{3+}.

The Au_2 cluster supported on the surface of CeO_2 with an oxygen vacancy and two peroxide species (Au_2–$(PO_2)_2$–V), has two stable adsorption structures: the Au_2 cluster is located perpendicularly (P) to the surface (Au_2–$(PO_2)_2$–V-P, Fig. 3i) and Au_2 lies parallel (L) to the surface (Au_2–$(PO_2)_2$–V-L, Fig. 3e). Their adsorption energies are 0.58 eV and 2.65 eV, respectively. Thus, we did not consider the perpendicular structure (Au_2–$(PO_2)_2$–V-P) in the following electronic analysis and CO oxidation.

As shown in the charge density difference of Au_2–$(PO_2)_2$–V-L in Fig. 3f, the surface oxygen vacancy leads to formation of two Ce^{3+} ions. As the peroxide interacted with the Au_2 cluster, the O–O bond was elongated from 1.44 Å to 1.48 Å, and the electron transfer from peroxide to gold results in the formation of a weak $Au^{\delta-}$ species. These results agreed with the Bader charge analysis (Table 2, −0.05*e*/−0.12*e*). Interestingly, this weak electronegative gold cluster can adsorb a CO molecule, as shown in Fig. 3g. When CO has access to the Au_2 cluster, the distance between Au and $O_{peroxide}$ is about 2.24 Å and 3.28 Å. The CO adsorption energy is 0.51 eV. The charge density difference analysis (Fig. 3h) shows that, the number of reduced Ce^{3+} is unchanged after CO adsorption, while an $Au^{\delta+}$ and an $Au^{\delta-}$ ion were formed, with charges +0.10*e* (Au_A) and −0.16*e* (Au_B), as shown in the Bader charge data (Table 2). It is interesting that CO interaction is more favorable on this Au_2 with $Au^{\delta-}$ than on $Au_1{}^{\delta-}$. We now explore the possibility that Au_3 or Au_4 that can accommodate $Au^{\delta-}$ will be more active towards CO adsorption.

3.3. Au_3 and Au_4 clusters adsorbed on the $CeO_2(111)$ surface and CO adsorption

For Au_3 clusters supported on the reduced $CeO_2(111)$ (CeO_2–$(PO_2)_y$–V_m) surface, the structure of Au_3–$(PO_2)_3$–V_1 is shown in Fig. 4a, and the structure of Au_3–$(PO_2)_2$–V_1 is shown in Fig. S3 (ESI†). As shown in Fig. 4a, the Au_3 cluster forms a triangular figure and its center is located at the top of the O vacancy, in which every Au atom is anchored by a peroxide. The distances between the Au and the $O_{peroxide}$ are 2.09, 2.22 and 2.14 Å, respectively. The lengths of the three Au–Au bonds are 2.65, 2.61, 2.74 Å. After CO adsorption on the Au_3 cluster (Au_3–$(PO_2)_3$–V_1, Fig. 4c), the distances of the Au–$O_{peroxide}$ changed to 2.11, 2.15 and 2.97 Å. The corresponding adsorption energy is 0.80 eV. To further analyze the electronic interactions between the adsorbate and the $CeO_2(111)$ facet, we calculated the charge density difference for the Au_3–$(PO_2)_3$–V_1 structure (Fig. 4b) and CO adsorption on its surface (Fig. 4d). Fig. 4b shows an electron transfer from the Au_3 cluster to a surface Ce; $Au - e \rightarrow Au^{\delta}+$, $Ce^{4+} + e \rightarrow Ce^{3+}$. Hence, there are three Ce^{3+} ions on the surface, and the positive charge of the Au atoms are obtained by computing the Bader charges to be +0.07*e*, +0.03*e* and +0.17*e*, respectively (Table 3). Furthermore, the Au-d band and the O-2p band of the O atom in the peroxide are overlapped, and we found that part of an electron transfers from Au_3 to peroxide. These results show that ceria has the capacity for storing electrons. In comparison with the adsorption of Au_1 and Au_2 on ceria, for the adsorption of Au_3, the ability of ceria for storing electrons is better to prevent the formation of negatively charged adsorbed Au_3, to help its reaction with CO. After CO adsorption, the number of Ce^{3+} ion is unchanged, and the charges of Au atoms are changed to +0.23*e*, +0.05*e* and +0.09*e* (Table 3) respectively. This shows that, after CO adsorption, the charge redistribution occurred in the Au/CeO_2 and CO/Au interfaces, where the electrons transferred from peroxide (close to CO) feedback to the Au_3, and from the Au_3 cluster to CO.

For Au_4 clusters supported on the reduced $CeO_2(111)$ facet (Au_4–$(PO_2)_3$–V_1), its configurations are shown in Fig. 4e, and the configurations of Au_4–$(PO_2)_4$–V_2 are shown in Fig. S3c (ESI†). The results show that, the Au_4 cluster forms a pyramidal structure, and is located at the top of the surface oxygen vacancy, in which its adsorption energy is 2.84 eV (Table 3). After CO adsorbed on Au_4/CeO_2 (($(PO_2)_3$–V_1) (Fig. 4g), the bond lengths of C–O and Au–C in the CO adsorption structure are ~1.15 and 1.94 Å respectively, and its adsorption energy was calculated to be 1.44 eV. The charge density difference analysis of Au_4–$(PO_2)_3$–V_1 (Fig. 4f) shows that, each peroxide interacts with one Au atom in the bottom layer, resulting in the electron transfer from peroxide O-2p states to Au-d states. In addition, the electrons of the Au atoms are transferred to the substrate, three reduced Ce^{3+} ions existed on the Au_4–$(PO_2)_3$–V_1 surface, and the charges of Au atoms were estimated by Bader charge to be −0.09*e*, +0.08*e*, +0.09*e* and +0.21*e*, respectively (Table 3).

As shown in Fig. 4g, CO is attached to Au_A (−0.09*e*/slight electronegative, Table 3). However, the $Au^{\delta-}$ ion is inactive for CO adsorption, and the electrons of the Au atoms are transferred through the peroxide to substrate Ce, the number of the partially reduced Ce^{4+} ions is now four (Fig. 4h). At the same time, CO also gets ~0.06*e* from Au. The lengths of Au–$O_{peroxide}$ bonds are unchanged. The Bader charges of Au atoms are calculated to be +0.26*e*, +0.08*e*, +0.07*e* and +0.10*e*, respectively, which is consistent with the results of the charge density difference (Fig. 4h).

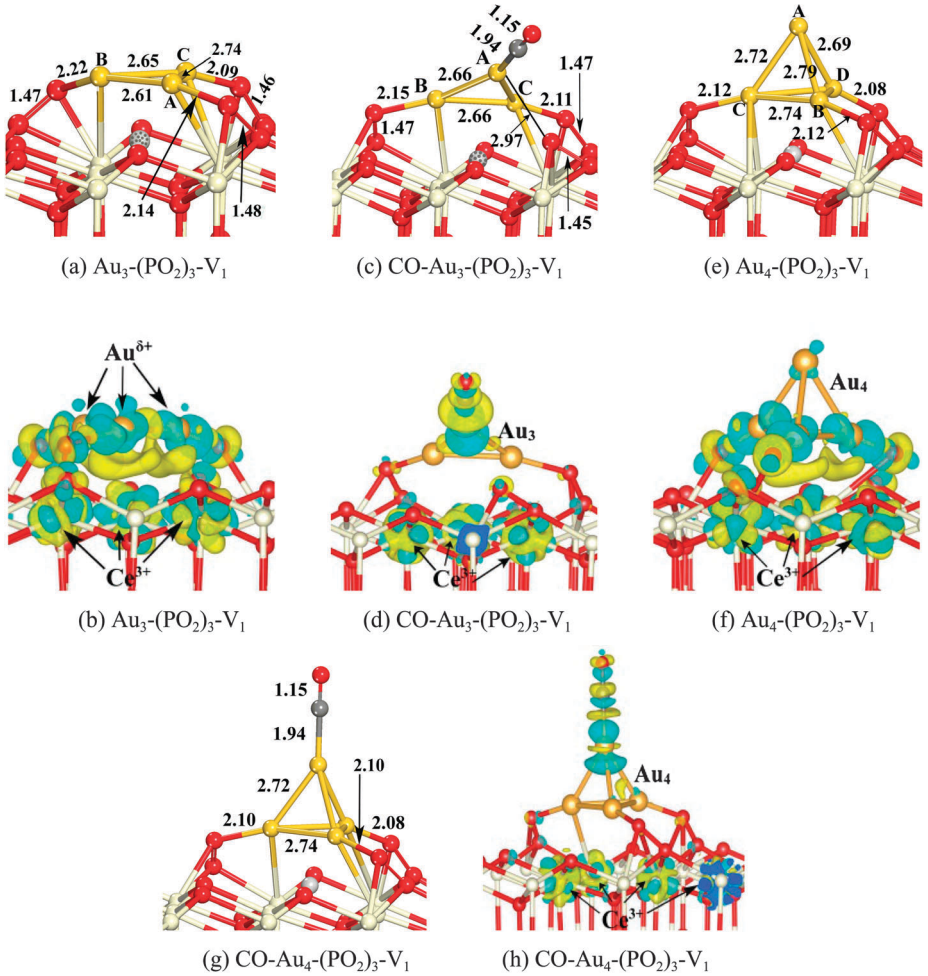

Fig. 4 Optimized structures of (a) Au_3 and (e) Au_4 clusters on the CeO_2(111) facet and CO adsorption on (c) Au_3/CeO_2(111) and (g) Au_4/CeO_2(111), and (b, d, f and h) the corresponding charge density differences. (O, Ce, Au, C atoms are denoted in red, gray, yellow and dark gray, respectively. The O vacancy is represented by balls in light gray. Main bond lengths (Å) are reported. Electron accumulation and depletion are represented by yellow and blue areas, respectively. The isosurface value is set as 0.005 e $Å^{-3}$.)

Table 3 The Au_3 and Au_4 clusters or CO adsorption (eV) and the Bader charge

		Au-Bader charge/*e*				CO-Bader charge/*e*
	E_{ad}/eV	Au_A	Au_B	Au_C	Au_D	
Au_3–$(PO_2)_3$–V_1	3.94	+0.07	+0.03	+0.17		
CO–Au_3–$(PO_2)_3$–V_1	0.80	+0.23	+0.05	+0.09		−0.04
Au_4–$(PO_2)_3$–V_1	2.84	−0.09	+0.08	+0.09	+0.21	
CO–Au_4–$(PO_2)_3$–V_1	1.44	+0.26	+0.08	+0.07	+0.10	−0.06

For the Au_4–$(PO_2)_4$–V_2 configuration (Fig. S3c, ESI†), all Au atoms lie on the surface with two structures of Au_2–$(PO_2)_2$–V_1-L. The Au_4 adsorption energy is 5.00 eV. CO can chemically adsorb on the supported Au_4 (Au_4–$(PO_2)_4$–V_2) with the adsorption energy of 0.57 eV.

The research results for Au_3 and Au_4 clusters further validate that, CeO_2 structures containing both peroxide and a vacancy (CeO_2–$(PO_2)_y$–V_m) help Au cluster adsorption/attachment on the CeO_2(111) facet. With increasing Au atoms in the Au clusters over CeO_2–$(PO_2)_y$–V_m, CO adsorption on this surface would be stronger than Au_1 and Au_2, in which CeO_2 acted as the electron buffer during both Au adsorption on CeO_2 and CO adsorption on Au_x/CeO_2.

3.4. Density of states

The typical density of states (DOS) for Au_1–$(PO_2)_1$ and CO adsorbed on Au_1–$(PO_2)_1$ configurations are shown in Fig. 5. Comparing with the DOS of the PO_2 and Au–PO_2, we found that two new features (labeled "A" and "B") appeared in the Au–PO_2 structure. For the Au–PO_2 structure, the filled Ce-4f band appeared between −1 and 0 eV (the A feature), which reveals that one Ce^{4+} is reduced to a Ce^{3+} ion, obviously, the electron transfer from Au to ceria through the Au–$O_{lattice}$ bond. Therefore, the overlapping between Au and $O_{lattice}$ gives rise to the C peak at −6 to −5 eV. The feature B is related to the Au–$O_{peroxide}$ bonding at −8 to −7 eV, it reveals that the Au–$O_{peroxide}$ bond results mostly from the overlap of Au-d states and the O-p states in peroxide. Based on the analysis of charge density difference,

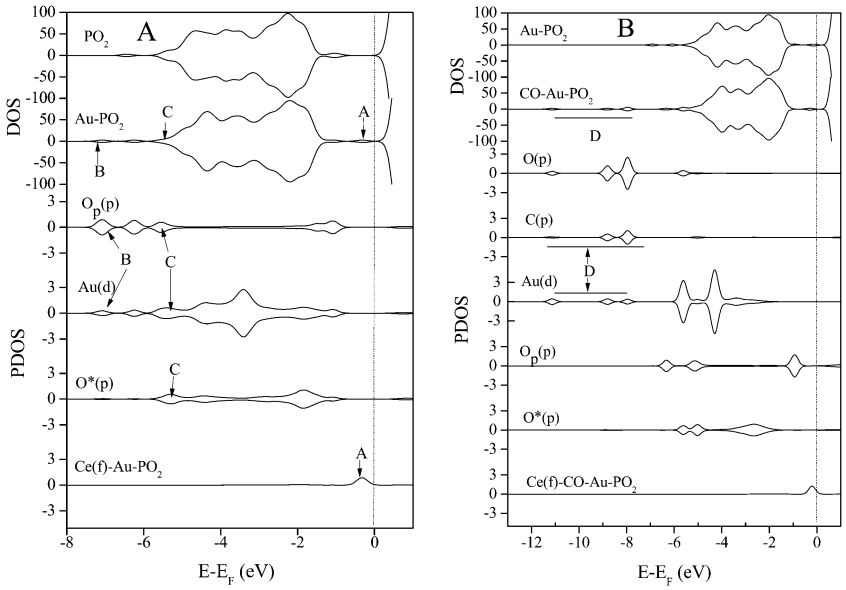

Fig. 5 Density of states of (A) Au_1–$(PO_2)_1$ and (B) CO–Au_1–$(PO_2)_1$ and their projected DOS analyses. The vertical dashed line indicates the Fermi level at 0 eV. (O – O atom in CO; O_p – O atom in peroxide; O* – lattice O.)

this is due to electron transfer from Au to O. After CO adsorption, the distance between Au and $O_{peroxide}$ is extended to 3.06 Å (Fig. 2c), indicating that there is little interaction between them. The charge of the $Au^{\delta+}$ transferred to the C atom and fed back to peroxide at the CO/Au and Au/CeO_2 interfaces or contacts, respectively. The overlapping of Au-d states and the C-p states results in the D feature at −11 to 7 eV in Fig. 5B.

On the basis of DOS, we can see, when Au is supported on a CeO_2–$(PO_2)_1$ surface, the charge would transfer in the following order: $PO_2 \rightarrow Au \rightarrow O_{lattice} \rightarrow Ce^{4+}$, $Ce^{4+} + Au^0 \rightarrow Ce^{3+} + Au^{\delta+}$, in which CeO_2 acts as an electronic buffer.

The DOS for Au_2–$(PO_2)_2$–V_1-L and CO–Au_2–$(PO_2)_2$–V_1-L is shown in Fig. 6. In Ce PDOS of $(PO_2)_2$–V, Au_2–$(PO_2)_2$–V and CO–Au_2–$(PO_2)_2$–V, two Ce^{3+} ions were formed and partially occupied electronic DOS peaks appeared at −2 to 0 eV. And the number of Ce^{3+} ions is unchanged during Au_2 or CO adsorption. There is no electron transfer between gold and the Ce^{3+}/Ce^{4+} ion. In comparison with $O_{peroxide}$ and Au PDOS of $(PO_2)_2$–V and Au_2–$(PO_2)_2$–V, the peaks of the similar B feature in Fig. 5A appear at −8 to −6 eV, which indicates the overlap between $O_{peroxide}$ and Au. Based on the analysis of the charge density difference and Bader charge, this is due to a few electrons from peroxide being transferred to the Au atom. As shown in Fig. 6B, when CO attached on Au_A, the B peak reduced greatly at −8 to −6 eV, while the new peak appeared around −10 eV, which results from the overlap of Au_A-d states and the C-p states. In addition,

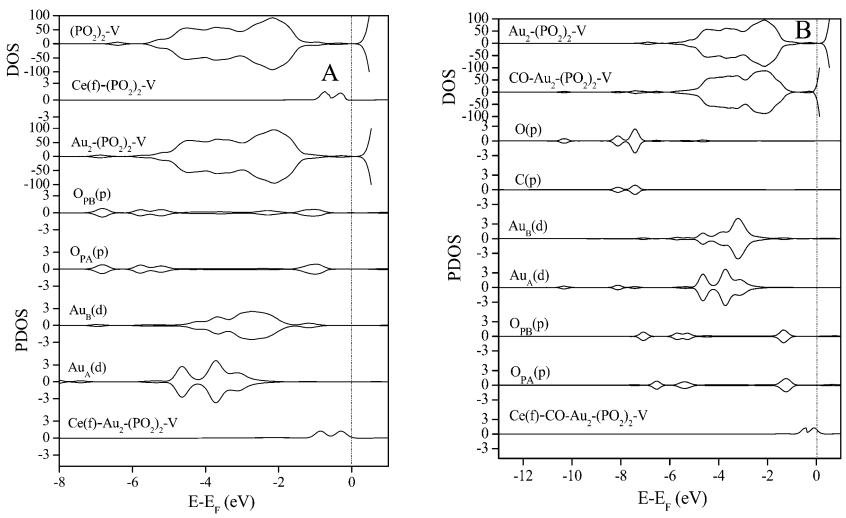

Fig. 6 Density of states of (A) Au_2–$(PO_2)_2$–V_1-L and (B) CO–Au_2–$(PO_2)_2$–V_1-L and their projected DOS analyses. The vertical dashed line indicates the Fermi level at 0 eV. (O – O atom in CO; O_p – O atom in peroxide; in Au_2–$(PO_2)_2$–V_1-L and CO–Au_2–$(PO_2)_2$–V_1-L configurations, Au_A connected to O_{PA} and Au_B connected to O_{PB}.)

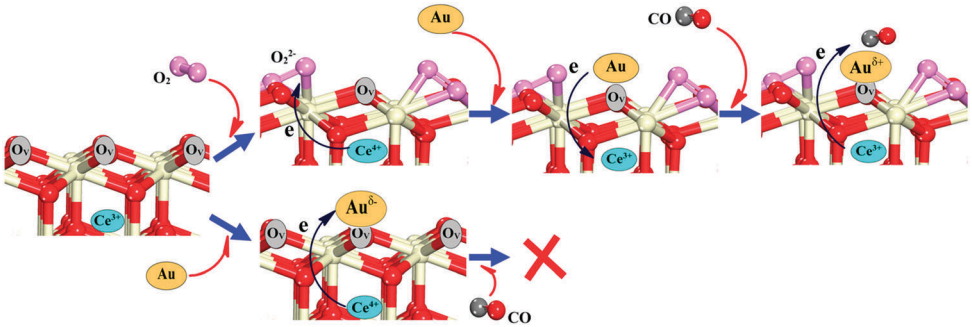

Scheme 1 Configurations of Au supported on CeO_2 with O vacancy or both peroxide and O vacancy, and CO adsorbed on Au/CeO_2.

the d orbitals of the two Au atoms are overlapped at −6 to −2 eV, which shows that the electrons transfer from Au_A to Au_B.

The DOS analysis show that charge transfers from peroxide to Au when Au_2 adsorbed on the $(PO_2)_2$–V_1-L surface, and Au-d states and $O_{peroxide}$-p states are overlapped. After CO adsorption, electrons feed from Au_A to peroxide, by way of the bond between Au_A and CO. So peroxide is an important species in Au_2 or CO adsorption.

3.5. Effect of peroxide on the reduced CeO_2(111) facet

Experimentally, using Raman spectroscopy, peroxide and superoxide species were characterized on the Au/CeO_2 surface,[23] and a correlation was found between the catalytic activity of gold and the peroxide and superoxide species. The formation of reactive oxygen species on the nanocrystalline support is enhanced by the gold.[32] Therefore, we studied Au adsorption around the peroxide. We simulated a structure in which only the boundary Au atom was active and the other gold atoms inert rather than each Au atom being anchored by a peroxide.

Au supported on ceria surfaces can be described as shown in Scheme 1. Oxygen vacancy is the common defect for most metal oxides. On ceria surfaces containing O vacancies the supported Au atom will become negatively charged.[24,28] $Au^{\delta-}$ ions are inactive for CO oxidation. Herein, our results show that O_2 adsorbed on a reduced CeO_{2-x}(111) facet (formed peroxide) can transfer the charge from $Au^{\delta-}$ ions to the peroxides. The negative charge of the Au_x cluster adsorbed on the CeO_2–$(PO_2)_y$–V_m surface is lower than that on CeO_2 with only oxygen vacancies, in which electrons transfer from the Au atom to the peroxide. The charges of Au_x ($x > 1$) on the CeO_2–$(PO_2)_y$–V_m surface are close to either slightly negatively charged or even slightly positively charged, which promotes CO adsorption on the Au_x/CeO_2 surface. When $x = 1$ (Au_1), the distance between the Au atom and $O_{peroxide}$ is 3.51 Å, there are no electron transfers from the Au atoms to the peroxide.

On the basis of the charge density difference, the Bader charge analyses and the results mentioned above we find ceria has the strong capability for electron storage. For example, when Au is supported on the upper site of the O vacancy on the CeO_2 surface (Fig. 1f), CeO_2 will transfer a removable electron to Au ($Ce^{3+} + Au^0 \rightarrow Ce^{4+} + Au^{\delta-}$). While for Au_x clusters ($x \geq 3$) supported on the surface of CeO_2 with peroxide and an O vacancy, the Au will transfer an electron to the CeO_2 substrate: $Ce^{4+} + Au^0 \rightarrow Ce^{3+} + Au^{\delta+}$. In short, CeO_2 acts as an electronic buffer.

4. Conclusions

In summary, by means of DFT+U calculations, we studied the adsorption behaviors of Au_x (x = 1–4) clusters on the various CeO_2(111) facets containing oxygen vacancies, peroxide and superoxide species. It has been found that, when Au_1 is supported on the CeO_2(111) facet with an O vacancy it forms a negatively charged $Au^{\delta-}$, and this is not favorable for CO adsorption on its surface. The structure of CeO_2(111) containing both an O vacancy and peroxide is stable and can effectively support the Au cluster (Au_x–$(PO_2)_y$–V_m), which enables Au supported on the CeO_2(111) facet to overcome Au–Au bond reunion.

On the basis of the charge density difference and Bader charge analyses, we further revealed the electron transfer mechanism. When Au_2 is supported on CeO_2 with two peroxides and one O vacancy (Au_2–$(PO_2)_2$–V_1), Au_2 is adsorbed strongly and parallel to the CeO_2–$(PO_2)_2$–V_1, electrons transfer from the peroxide to the supported Au atom to form weak $Au^{\delta-}$. However, this weakly negatively charged gold cluster can adsorb a CO molecule. When an Au_x cluster ($x \geq 3$) is supported on the surface of CeO_2 with peroxide and an O vacancy, Au will transfer an electron to the CeO_2 substrate. With an increasing number of Au atoms in the Au clusters adsorbed on CeO_2–$(PO_2)_y$–V_m, CO adsorption on the surface will be stronger. For both Au supported on CeO_2 and CO adsorbed on Au_x/CeO_2, CeO_2 acts as an electron buffer. The CeO_2 structures containing both peroxide and a vacancy (CeO_2–$(PO_2)_y$–V_m) help Au cluster adsorption/attachment on the CeO_2(111) facet, and CO adsorption was greatly improved, which sets the basic foundation for the next step: CO oxidation.

Acknowledgements

This project was financially supported by the National Natural Science Foundation of China (21273150, 21203119), the National Basic Research Program of China (2013CB933201), the national high technology research and development program of China (2011AA03A406, 2012AA062703), the Shanghai Natural Science Foundation (12ZR1430800), and the Shanghai Innovation Program (12YZ161).

Notes and references

1 P. Ghosh, M. F. Camellone and S. Fabris, *J. Phys. Chem. Lett.*, 2013, **4**, 2256.
2 F. Chen, D. Liu, J. Zhang, P. Hu, X.-Q. Gong and G. Lu, *Phys. Chem. Chem. Phys.*, 2012, **14**, 16573.
3 C. Liu, Y. Tan, S. Lin, H. Li, X. Wu, L. Li and Y. Pei, *J. Am. Chem. Soc.*, 2013, **135**, 2583.
4 F. Chen, J. Cheng, P. Hu and H. Wang, *Surf. Sci.*, 2008, **602**, 2828.
5 S. Zhang, X.-S. Li, B. Chen, X. Zhu, C. Shi and A.-M. Zhu, *ACS Catal.*, 2014, **4**, 3481.
6 Z. P. Liu, S. J. Jenkins and D. A. King, *Phys. Rev. Lett.*, 2005, **94**, 196102.
7 F. Vindigin, M. Manzoli, T. Tabakova, V. Idakiev, F. Boccuzzi and A. Chiorino, *Phys. Chem. Chem. Phys.*, 2013, **15**, 13400.
8 A. B. Vidal, L. Feria, J. Evans, Y. Takahashi, P. Liu, K. Nakamura, F. Illas and J. A. Rodriguez, *J. Phys. Chem. Lett.*, 2012, **3**, 2275.
9 C. Hamill, R. Burch, A. Goguet, D. Rooney, H. Driss, L. Petrov and M. Daous, *Appl. Catal., B*, 2014, **147**, 864.
10 T. D. Chau, T. Visart de Bocarme and N. Kruse, *Catal. Lett.*, 2004, **98**, 85.
11 C. P. Vinod, J. W. Niemantsverdriet Hans and B. E. Nieuwenhuys, *Appl. Catal., A*, 2005, **291**, 93.
12 J. Zhang, X. Q. Gong and G. Z. Lu, *Chin. J. Catal.*, 2014, **35**, 1305.
13 G. Pattrick, E. van der Lingen, C. W. Corti, R. J. Holliday and D. T. Thompson, *Top. Catal.*, 2004, **30–31**, 273.
14 M. Haruta, T. Kobayashi, H. Sano and N. Yamada, *Chem. Lett.*, 1987, 405.
15 M. Haruta, S. Tsubota, T. Kobayashi, H. Kageyama, M. J. Genet and B. Delmon, *J. Catal.*, 1993, **144**, 175.
16 M. Valden, X. Lai and D. W. Goodman, *Science*, 1998, **281**, 1647.
17 R. Meyer, C. Lemire, S. K. Shaikhutdinov and H. Freund, *Gold Bull.*, 2004, **37**, 72.
18 M. Haruta, *Faraday Discuss.*, 2011, **152**, 11.
19 N. Ta, F. Wang, H. Li and W. Shen, *Catal. Today*, 2011, **175**(1), 541.
20 N. Ta, J. Liu, S. Chenna, P. A. Crozier, Y. Li, A. Chen and W. Shen, *J. Am. Chem. Soc.*, 2012, **134**, 20585.
21 S. Chen, L. Luo, Z. Jiang and W. Huang, *ACS Catal.*, 2015, **5**, 1653.
22 P. Concepción, S. Carrettin and A. Corma, *Appl. Catal., A*, 2006, **307**, 42.
23 J. Guzman, S. Carrettin and A. Corma, *J. Am. Chem. Soc.*, 2005, **127**, 3286.
24 M. F. Camellone and S. Fabris, *J. Am. Chem. Soc.*, 2009, **131**, 10473.
25 A. M. Venezia, P. Giuseppe, A. Longo, G. Di Carlo, M. P. Casaletto, F. L. Liotta and G. Deganello, *J. Phys. Chem. B*, 2005, **109**, 2821.
26 C. Zhang, A. Michaelides, D. A. King and S. J. Jenkins, *J. Phys. Chem. C*, 2009, **113**, 6411.
27 N. C. Hernández, R. Grau-Crespo, N. H. de Leeuw and J. F. Sanz, *Phys. Chem. Chem. Phys.*, 2009, **11**, 5246.
28 T. Tabakova, F. Boccuzzi, A. Chiorino, M. Manzoli and D. Andreeva, *Appl. Catal., A*, 2003, **252**, 385.
29 S. Carrettin, P. Concepción, A. Corma, J. M. López Nieto and V. F. Puntes, *Angew. Chem., Int. Ed.*, 2004, **43**, 2538.
30 X.-S. Huang, H. Sun, L.-C. Wang, Y.-M. Liu, K.-N. Fan and Y. Cao, *Appl. Catal., B*, 2009, **90**, 224.
31 C. Pan, D. Zhang, L. Shi and J. Fang, *Eur. J. Inorg. Chem.*, 2008, 2429.
32 J. Guzman, S. Carrettin, J. C. Fierro-Gonzalez, Y. Hao, B. C. Gates and A. Corma, *Angew. Chem., Int. Ed.*, 2005, **44**, 4778.
33 A. Martínez-Arias, J. Conesa and J. Soria, *Res. Chem. Intermed.*, 2007, **33**, 775.
34 C. Li, K. Domen, K.-I. Maruya and T. Onishi, *J. Catal.*, 1990, **123**, 436.
35 Y. M. Choi, H. Abernathy, H.-T. Chen, M. C. Lin and M. Liu, *ChemPhysChem*, 2006, **7**(9), 1957.
36 V. V. Pushkarev, V. I. Kovalchuk and J. L. d'Itri, *J. Phys. Chem. B*, 2004, **108**, 5341.
37 Z. Wu, M. Li, J. Howe, H. M. Meyer and S. H. Overbury, *Langmuir*, 2010, **26**, 16595.
38 H.-Y. Li, H.-F. Wang, X.-Q. Gong, Y.-L. Guo, Y. Guo, G. Lu and P. Hu, *Phys. Rev. B: Condens. Matter Mater. Phys.*, 2009, **79**(19), 193401.
39 M. Huang and S. Fabris, *Phys. Rev. B: Condens. Matter Mater. Phys.*, 2007, **75**(8), 081404.
40 Y. Zhao, B.-T. Teng, X.-D. Wen, Y. Zhao, Q.-P. Chen, L.-H. Zhao and M.-F. Luo, *J. Phys. Chem. C*, 2012, **116**, 15986.
41 W. J. Zhu, J. Zhang, X. Q. Gong and G. Z. Lu, *Catal. Today*, 2011, **165**(1), 19.
42 H. Y. Kim and G. Henkelman, *J. Phys. Chem. Lett.*, 2012, **3**, 2194.
43 H. Y. Kim, H. M. Lee and G. Henkelman, *J. Am. Chem. Soc.*, 2012, **134**, 1560.
44 H.-F. Wang, X.-Q. Gong, Y.-L. Guo, Y. Guo, G. Z. Lu and P. Hu, *J. Phys. Chem. C*, 2009, **113**, 10229.
45 Z. Yang, T. K. Woo and K. Hermansson, *J. Chem. Phys.*, 2006, **124**, 224704.
46 W. Song and E. J. M. Hensen, *ACS Catal.*, 2014, **4**, 1885.
47 S. M. Kozlov and K. M. Neyman, *Phys. Chem. Chem. Phys.*, 2014, **16**, 7823.
48 W. Cen, Y. Liu, Z. Wu, H. Wang and X. Weng, *Phys. Chem. Chem. Phys.*, 2012, **111**, 1.
49 M. M. Branda, N. C. Hernández, J. F. Sanz and F. Illas, *J. Phys. Chem. C*, 2010, **114**, 1934.
50 M. M. Branda, R. M. Ferullo, M. Causá and F. Illas, *J. Phys. Chem. C*, 2011, **115**, 3716.
51 M. M. Branda, C. Loschen, K. M. Ney man and F. Illas, *J. Phys. Chem. C*, 2008, **112**, 17643.
52 G. Kresse and J. Hafner, *Phys. Rev. B: Condens. Matter Mater. Phys.*, 1994, **49**, 14251.
53 G. Kresse and J. Furthmuller, *Phys. Rev. B: Condens. Matter Mater. Phys.*, 1996, **54**, 11169.
54 G. Kresse and D. Jouber, *Phys. Rev. B: Condens. Matter Mater. Phys.*, 1999, **59**, 1758.
55 O. Bengone, M. Alouani, P. Blochl and J. Hugel, *Phys. Rev. B: Condens. Matter Mater. Phys.*, 2000, **62**, 16392.

56 S. Fabris, S. de Gironcoli, S. Baroni, G. Vicario and G. Balducci, *Phys. Rev. B: Condens. Matter Mater. Phys.*, 2005, **71**, 041102.
57 M. Nolan, S. Grigoleit, S. C. Parker and G. W. Watson, *Surf. Sci.*, 2005, **576**, 217.
58 M. Nolan, S. C. Parker and G. W. Watson, *Surf. Sci.*, 2005, **595**, 223.
59 M. Nolan, S. C. Parker and G. W. Watson, *J. Phys. Chem. B*, 2006, **110**, 2256.
60 C. Zhang, A. Michaelides, D. A. King and J. J. Stephen, *J. Chem. Phys.*, 2008, **129**(19), 194708.
61 C. Zhang, A. Michaelides, D. A. King and J. J. Stephen, *J. Am. Chem. Soc.*, 2010, **132**(7), 2175.
62 Z. K. Han and Y. Gao, *Nanoscale*, 2015, **7**(1), 308.
63 W. Song and E. J. M. Hensen, *J. Phys. Chem. C*, 2013, **117**(15), 7721.
64 N. J. Castellani, M. M. Branda and K. M. Neyman, *J. Phys. Chem. C*, 2009, **113**(12), 4948.
65 L. Cui, Y. Tang, H. Zhang, L. G. Hector Jr., C. Ouyang, S. Shi, H. Li and L. Chen, *Phys. Chem. Chem. Phys.*, 2012, **14**, 1923.
66 Y. Chen, P. Hu, M.-H. Lee and H. Wang, *Surf. Sci.*, 2008, **602**, 1736.
67 B. Teng, F. Wu, W. Huang, X. Wen, L. Zhao and M. Luo, *ChemPhysChem*, 2012, **13**, 1261.
68 F. Esch, S. Fabris, L. Zhou, T. Montini, C. Africh, P. Fornasiero, G. Comelli and R. Rosei, *Science*, 2005, **309**, 752.
69 C. Zhang, A. Michaelides, D. A. King and S. J. Jenkins, *Phys. Rev. B: Condens. Matter Mater. Phys.*, 2009, **79**, 075433.

